Feasibility of tracking multiple implanted magnets with a myokinetic control interface: simulation and experimental evidence based on the point dipole model

Sergio Tarantino†, Francesco Clemente†*, Antonio De Simone and Christian Cipriani, *Senior Member, IEEE*

***Abstract*— *Objective:* The quest for an intuitive and physiologically appropriate human-machine interface for the control of dexterous prostheses is far from being completed. To control a hand prosthesis, a possible approach could consist in using information related to the displacement of forearm muscles of an amputee during contraction. We recently proposed that muscle displacement could be monitored by implanting passive magnetic markers (MMs – i.e. permanent magnets) in them. We dubbed this the *myokinetic interface*. However, besides the system feasibility, how much its accuracy, precision and computation time are affected by the number and distribution of both the MMs and the sensors used to record the MF was not quantified. *Methods:* Here we investigated, through simulations validated with a physical system, the performance of a system capable to track position and orientation of up to 9 MMs using information from up to 112 sensors in a volume resembling the dimensions of the human forearm. *Results:* The system was able to track up to 7 MMs in 450ms, demonstrating position/orientation accuracies in the range of 1mm/5°. The comparison with the experimental recordings demonstrated a median difference with the simulations in the order of 0.45mm. *Conclusion:* We were able to formulate general guidelines for the implementation of magnetic tracking systems. *Significance:* Our results pave the way towards the development of new human-machine interfaces for the control of artificial limbs, but they are also interesting for the whole range of biomedical engineering applications exploiting magnetic tracking.**

***Index Terms*—myokinetic interface, upper limb prosthetics, human-machine interface, simulation, magnetic field, Levenberg-Marquardt, magnetic tracking**

I. Introduction

MAGNETIC tracking deals with the determination of the position and/or orientation of a specially designed marker or device by means of its interaction with static or low-frequency magnetic fields [1]. This concept has been investigated by several groups over the last decades in a number of biomedical and industrial applications. As a representative example, the scleral search coil method for eye tracking, introduced by Robinson in the 60s [2] and refined by Collewijn *et al.* [3] is still considered one of the gold standards in oculomotor and neuroscience research [4]. Eye position is determined by placing a coil of thin copper wire in the eye. When the subject is placed in an AC magnetic field, the position of the eye can be determined from the amplitude of the induction current in the coil, with high spatial and temporal resolutions. Other biomedical applications include tracking of body [5], [6] and bone movements [7]–[9], of surgical needles [10], [11], catheters or steerable needles [12], and more complex instruments like bronchoscopes [13], colonoscopes and endoscopes [14]–[22]. A comprehensive review of magnetic tracking systems, including those for non-medical applications, was recently presented by Pasku *et al.* [23]. The reason for the popularity of magnetic tracking within biomedical engineering is that the human body is transparent to low-frequency magnetic fields. Therefore, the signal read by the tracking system is not affected by variable details of the human anatomy. In addition, if compared to optical methods, magnetic tracking does not require a free line-of-sight between the markers and the tracker [24], which makes it advantageous for intra-body applications [25].

Magnetic tracking systems exploit either static magnetic fields [8], [15], or low-frequency alternating magnetic fields [6], [11]. In the static case, permanent magnets are normally used as sources for the magnetic field and the field they generate is measured by Hall sensors [8], [26]; whereas, in the case with alternating fields, coils are usually used as the sources. The object to be tracked is often equipped with a sensor that is exposed to the field produced by one or multiple sources [16]. However, several systems are operated in the reversed manner. Consequently, the position and orientation (namely, the pose) of one or multiple sources is determined by measuring the field they generate with several sensors. Then, an inverse problem is solved to reconstruct the pose of the sources [1], [25]. One of the main advantages in tracking

†Equal contribution

This work was supported by the European Research Council under the MYKI project (ERC-2015-StG, Grant no. 679820).

All authors are with The BioRobotics Institute and with the Department of Excellence in Robotics & AI, Scuola Superiore Sant'Anna, Pisa, Italy. (correspondence e-mail: f.clemente@santannapisa.it).

permanent magnets rather than coils is that they are passive, and thus they neither require a power supply nor wires to generate the magnetic field. Hence, this represents a candidate solution in those cases where a (wireless) implanted device needs to be tracked [4], [8], [9]. In the following, we refer to such architecture.

We recently proposed a new concept of human-machine interface for the control of artificial limbs, particularly promising for hands, which takes advantage of the new opportunities offered by the tracking approach described above, termed *myokinetic control interface* [27], [28]. The idea is to use multiple permanent magnets (magnetic markers: MMs) implanted in the residual forearm muscles of an upper limb amputee to track the physical displacements of those muscles during contraction. Indeed, since each MM would travel with the muscle it is implanted in, its tracking would provide a direct measure of the contraction/elongation of that muscle. This information can then be used to control, proportionally and independently, the force/position of the relative movement in a hand prosthesis (so called amplitude-modulated control [29]). In particular, the ability of localizing multiple MMs would allow to monitor the contractions of several muscles, allowing simultaneous control over multiple movements in the hand prosthesis. This represents an important goal in the field and is currently only possible with implantable myoelectric sensors (IMES) –i.e., active devices– which record the electrical activity associated to muscle contraction [30]–[32].

Most of the permanent magnet tracking systems developed so far reconstruct the pose of a single marker using a suitable number of Hall sensors [8], [9], [26], [33]. The problem of reconstructing the pose of a magnet from measurements of the field it generates is called the inverse problem of magnetostatics. When the magnet is modelled as a point dipole, it is a mathematical problem with 5 unknowns (or degrees of freedom – DoFs – 3 for position and 2 for orientation) which can be solved if enough data on the generated magnetic field are available, e.g., with measurements from at least two 3-axis magnetic sensors or five 1-axis sensors [33]. Few exceptions to single marker systems are the trackers developed by Yabukami *et al.* [34], Yang *et al.* [35], and Tarantino *et al.* [27], that considered the pose of two (10 DoFs) and three markers (15 DoFs), and the position of four markers (12 DoFs), respectively. However, systems capable to track many more magnets are yet not available and represent an opportunity which may enable a new class of biomedical applications.

In view of this background, we investigated the limits of a multi-magnet tracking system, in a workspace/volume resembling the dimensions and geometries of the human forearm, using magnets small enough for implantation. The viability of the myokinetic control interface, and –generally speaking– of magnetic tracking systems, depends on a number of factors including: the volume of the workspace w.r.t. the strength of the magnetic field produced by the MMs [22], the approximations used in the modelling of such field [36] and in the numerical solver of the inverse problem [33], the number of MMs [34], the number and the layout of the sensors [1], [17], [22], [35], [37], their resolution and precision [17], [22], [33], and other environmental factors [27], [35]. Indeed, since the magnetic field of a MM drops off rapidly, with the inverse cube of distance, large distances may compromise the discriminating power of the sensors, while the closer a MM is to the sensors, the less accurate is the point dipole model. In addition, since numerical solvers reach more accurate solutions when the number of equations is much larger than the number of unknowns, the tracking accuracy improves with the number of sensors [17], [22], [33], [37].

In order to quantify some of these effects, in this study we investigated the viability and the performance of a multi-magnet tracking system capable to track up to 9 MMs. In particular, the impact on pose tracking accuracy and on computation time of (i) the number of MMs, (ii) the shape of the MMs, (iii) the number of sensors, and (iv) the electrical noise, were simulated numerically and validated experimentally. All together the results prove the feasibility of a system tracking up to 7 MMs (35 DoFs) and provides insights on its possible theoretical and practical limitations. In fact, 9 MMs could neither be tracked with reasonable accuracy nor fast enough for ensuring online operation. The simulated results demonstrated compound/cumulative accuracies in the ranges of 1 mm and 5° for 7 MMs and cross-talk and noise errors in similar ranges, for two shapes of MMs. As expected the distance of the MM to the sensors proved significantly (inversely) correlated with the accuracy, while the computation time proved proportional to both the number of sensors and MMs. The comparison with the experimental recordings demonstrated a median difference with the simulations in the order of ~0.45 mm. These outcomes are of interest for a range of bioengineering applications in which remote tracking is necessary and support the idea of permanent magnets implanted in the residual muscles to achieve highly dexterous control of hand prostheses.

II. Materials and Methods

The magnetic field $\boldsymbol{B}$ generated by multiple (say, n) MMs moving in space, each uniformly magnetized, is described by the solution of the direct problem of magnetostatics:

$$\boldsymbol{B}(x) = \mu_0 \left(-\nabla V_m(x) + \sum_{j=1}^{n} \boldsymbol{M}_j \chi_{\Omega_j}(x) \right) \quad (1)$$

where μ_0 is the magnetic permittivity of vacuum, Ω_j is the region of space occupied by the j-th MM, χ_{Ω_j} its characteristic function such that $\chi_{\Omega_j}(x) = 1$ if $x \in \Omega_j$ and $\chi_{\Omega_j}(x) = 0$ otherwise, and $\boldsymbol{M}_j$ its constant magnetization. Moreover, V_m is the magnetic scalar potential obtained as the solution of $\nabla \cdot \boldsymbol{B} = 0$ in the whole 3D space containing the MMs, namely,

$$V_m = \Delta^{-1} \left(\nabla \cdot \left(\sum_{j=1}^{n} \boldsymbol{M}_j \chi_{\Omega_j} \right) \right) \quad (2)$$

We used a Finite Element software package (Comsol Multiphysics, COMSOL Inc., Stockholm, Sweden) to

numerically solve (1) and (2), in order to accurately simulate the magnetic field produced by *n* MMs moving in the space. The field was then sampled at N locations, and fed to a Matlab R2016a script (MathWorks, Natick, MA) that ran a localization algorithm, which allowed for the offline estimation of the pose of the MMs by solving the inverse magnetostatic problem. 400 setups, mixing different (in terms of number and shape) MMs, trajectories, and sensing options, were simulated in order to assess the localization errors. Finally, the results of the simulations were validated by comparing them with those achieved on a physical demonstrator.

A. Mathematical approximations and localization algorithm

In order to simplify the solution of the localization problem (inverse problem of magnetostatics) the magnetization field, which is constant over each of the *n* MMs and zero away from them, can be approximated as a collection of *n* point magnetic dipoles, each located at the center of one MM. The magnetic field $\boldsymbol{B}_i = \boldsymbol{B}(x_i)$, generated at the location $\boldsymbol{x}_i$ by a collection of *n* dipoles located at $\boldsymbol{x}_j$, j=1, …, n, with magnetic moment respectively equal to $M\widehat{\boldsymbol{m}_j}$ (here M and $\widehat{\boldsymbol{m}_j}$ are the magnitude and direction of the magnetic moment of the j-th MM) can be evaluated as

$$\boldsymbol{B}_i = \boldsymbol{B}(x_i) = \sum_{j=1}^{n} \frac{M_j \mu_r \mu_0}{4\pi} \left(\frac{3(\widehat{\boldsymbol{m}_j} \cdot \boldsymbol{x}_{ij}) \boldsymbol{x}_{ij}}{|\boldsymbol{x}_{ij}|^5} - \frac{\widehat{\boldsymbol{m}_j}}{|\boldsymbol{x}_{ij}|^3} \right), \text{i=1,…,N} \quad (3)$$

Here $\boldsymbol{x}_{ij} = \boldsymbol{x}_i - \boldsymbol{x}_j$ and $\boldsymbol{x}_i$ represent the locations of N sites (sensors) where the magnetic field is assumed to be known or measurable. Eq. (3) is obtained by adding the field generated by each dipole where we recall that, for a dipole of magnetic moment $M\,\widehat{\boldsymbol{m}}$ located at the origin, the magnetic field at $\boldsymbol{x}_i$ is given by

$$\boldsymbol{B}_i = \boldsymbol{B}(x_i) = \frac{M \mu_r \mu_0}{4\pi} \left(\frac{3(\widehat{\boldsymbol{m}} \cdot \boldsymbol{x}_i) \boldsymbol{x}_i}{|\boldsymbol{x}_i|^5} - \frac{\widehat{\boldsymbol{m}}}{|\boldsymbol{x}_i|^3} \right) \quad (4)$$

Eq. (3), in which the geometry of the MMs (i.e. χ_{Ω_j}) no longer plays a role, provides a good approximation for the magnetic field generated by the MMs, which is better represented by the solution of (1). The approximation is excellent in the ideal case of infinite distance between sensors and sources (far field) and it loses accuracy when this distance becomes smaller [36]. Nevertheless, this *point dipole approximation* proves sufficiently accurate in several non-ideal cases [18]–[20], [26], including the myokinetic control interface.

Solving the N Equations (3) with respect to $\boldsymbol{x_j}$ and $\boldsymbol{m}$ provides the localization (position and orientation estimation) of *n* MMs. Solving this inverse problem provides the input data required for the myokinetic control interface; however, as there is no closed form solution, the latter can only be obtained by numerical approximation. In addition, for a myokinetic control interface, the absolute pose of a MM is not informative alone of the status of the contraction of a residual muscle. It is the displacement of the MM from an offset pose (recorded with uncontracted, relaxed muscles) that reveals the degree of contraction of the muscle it is implanted in.

The inaccuracies in the point dipole approximation and those introduced when solving the equations numerically may cause errors in estimating the displacement of single magnets (e_m) and can yield to false predictions of simultaneous displacements (i.e. cross-talk – e_{ct}) in the case of multiple magnets. Notably, these errors depend on the geometrical configuration of MMs in the workspace. Thus, for a myokinetic control interface comprising *n* magnets, with 1 magnet moving at a time, and neglecting environmental factors [27], [35], its position error (E_d) and orientation error (E_o) at a certain pose p_x, can be described as:

$$\mathrm{E_d} = D_{est} - D_{act} \approx e_{\mathrm{m_d}}(p_x) + \sum_{j=1}^{n-1} e_{\mathrm{ct_d}\,j}(p_x) \quad (3)$$

$$\mathrm{E_o} = O_{est} - O_{act} \approx e_{\mathrm{m}_o}(p_x) + \sum_{j=1}^{n-1} e_{\mathrm{ct}_o\,j}(p_x) \quad (4)$$

where D_{est} and O_{est} are the estimated position and orientation displacements, and D_{act} and O_{act} are the actual values. Such a description stands for the ideal case. In the real case, measurement uncertainties come in, because the reading of $\boldsymbol{B}_i$ is affected by the non-ideal accuracy and repeatability of the sensing apparatus (technological limitations). This variability affects the estimation of e_m and e_{ct}, and can be taken into account with the following:

$$e_k(p_x) = \overline{e_k(p_x, s)} \pm S_k(p_x, s), k \in [m_d, m_o, ct_d, ct_o] \quad (5)$$

i.e. with an average value plus-minus a certain variability, *S*. Combining equations (3)-(5) we thus obtain for $\mathrm{E_d}$ (and similarly for $\mathrm{E_o}$):

$$\mathrm{E_d} \approx \overline{e_{m_d}(p_x, s)} \pm S_{m_d}(p_x, s) + \sum_{j=1}^{n-1} \left(\overline{e_{\mathrm{ct_d}\,j}(p_x, s)} \pm S_{ct_d}(p_x, s) \right) \quad (6)$$

where *s* represents the sensing apparatus. The four contributions in (6) can be estimated by imposing specific experimental conditions that nullify all of them except one, and knowing the theoretical and estimated position and orientation displacements. In particular, moving a single magnet at a time and resolving the inverse magnetic problem exposes its $\overline{e_{m_d}(p_x, s)}$; moving the other *n-1* magnets and keeping fixed the target one (at a rest pose) provides their cross-talk contribution on the error ($\sum_{j=1}^{n-1} \overline{e_{\mathrm{ct_d}\,j}(p_x, s)}$). Finally, repeating such measurements a number of times provides the contributions associated to measurement uncertainties, S_k, e.g. by using one standard deviation.

B. Simulation setup

Five systems, each comprising a different number of MMs (either 1, 3, 5, 7 or 9), in a fixed workspace, were simulated. The MMs were modeled as Nd-Fe-B N42 grade magnets (axial remanent magnetization B_r=1.45 T), while the workspace as a parallelepiped of 94 mm × 54 mm × 94 mm (*l* × *w* × *h*) with the bottom base centered in the origin of a

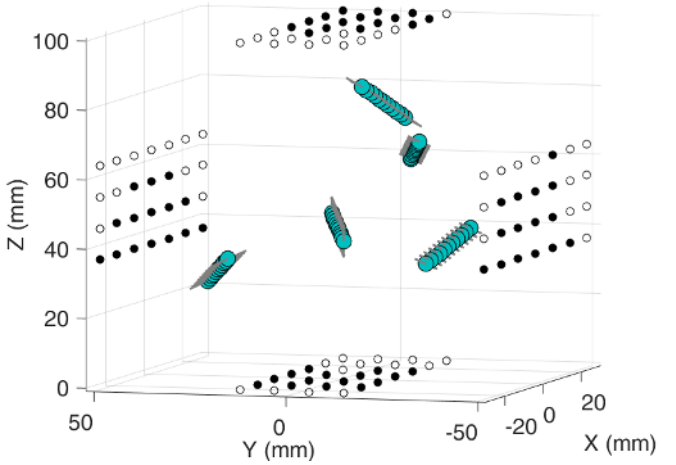

Fig. 1. Example of a set of simulated poses (position and orientation) randomly assigned during a five-MM simulation. Each MM was translated by a certain distance, one at a time, in order to mimic muscle contraction. Colored spheres represent MMs along their trajectories, grey lines represent the orientation of the magnetic moment, black dots on the external walls represent the 60 sites populated with a magnetic field sensor (active sites) in this configuration, while the empty dots indicate the other possible sites.

Cartesian coordinate system parallel to the XY plane at z = 0 (Fig. 1). The workspace dimensions mimicked those of a human forearm [38].

For each system, we simulated the movements of the MMs, each one along a pre-defined linear trajectory, having a starting (P_S) and an end point (P_F) enclosed in the workspace (Fig. 1). Both the starting and end points of the trajectories were semi-randomly chosen. In particular, the starting point was randomly chosen within the workspace (uniform distribution along X, Y and Z), whereas the end point was chosen in a way that the trajectory was fully contained in the workspace and the distance $\overline{P_S P_F}$ (i.e. the length of the trajectory) ranged between 10 mm and 20 mm (random selection with uniform distribution – Fig. 1). The movements of the MMs were simulated by assigning them positions and orientations and by translating them, one MM at a time, along the direction vectors of the trajectories to 11 equidistant checkpoints along the trajectory (0%, 10%, 20%, …, 100% of the length). At each checkpoint the (compound) magnetic field in the workspace was computed (numerical solution of (1) and (2)) and stored for offline localization of the MMs (Levenberg-Marquardt Algorithm [39] on (3), akin to our previous work [27]; initial guess set as the true pose of the MMs).

For each system, the above procedure was repeated four times (i.e. four trials). Each time a new set of semi-random trajectories was assigned to the MMs, thus giving rise to a completely different setup (maintaining only the number of MM). At each trial, the azimuthal and the elevation angle pair of each MM were randomly chosen within a predefined subset of angles (i.e. 0°, 15°, 30°, 45°, exploiting the symmetries of the workspace geometry).

The magnetic field was sampled at specific sites simulating the presence of magnetic field sensors. The sites were laid out on four planar and orthogonal grids (or groups) of seven columns and four rows (112 sites). Each column and row were separated by a 9 mm gap. The four groups were spatially

TABLE I
SIMULATION PARAMETERS SUMMARY (400 DIFFERENT SETUPS)

Number of trials	4
Number of MMs	1, 3, 5, 7, 9
Number of active sites	4, 8, 12, 16, 28, 40, 60, 80, 100, 112
Selection of active sites	Based on the strength of the magnetic field with the MMs in the starting position
Presence of noise	- Yes
Type of MM	- 3 mm diameter sphere (sMM) - 4 mm diameter and 2 mm height disc (dMM)

centered on four opposite sides of a parallelepiped enclosing the workspace (100 mm × 54 mm × 100 mm) (two on the XZ plane, two on the XY plane – Fig. 1). For each system, multiple configurations of "active" sites (i.e. sites populated by a sensor) were simulated. In particular, the configurations were generated by varying the number of active sites (i.e. 4, 8, 12, 16, 28, 40, 60, 80, 100 and 112), and choosing those recording the maximum strength of the magnetic field (measured when the MMs were in the starting position).

Furthermore, the simulations were performed by adding Gaussian noise on the sampled magnetic field (10 repetitions), in order to investigate the effects of measurement uncertainties on the overall performance. The Gaussian noise had a standard deviation of 0.004 G, corresponding to the noise characteristics measured on a commercial magnetometer (MAG3110, Freescale Semiconductor, Inc.). Finally, the four trials were repeated using two types of MMs: (i) spheres having a 3 mm diameter (sMM, M = 0.0163 Am^2) and (ii) discs having a 4 mm diameter and a 2 mm height (dMM, M = 0.029 Am^2). The combination of all the parameters resulted in 400 simulations (4 trials × 5 systems × 10 sensor populations × 2 MM types – Table 1).

C. *Performance evaluation*

The performance of the myokinetic control interface was quantified as measured by the localization errors in (6) (in both the position and orientation components), averaged across the trajectories within each system. In particular, for each system and each configuration of active (sensory) sites, the compound/cumulative $\overline{e_m}$ along the trajectories and across magnets, was computed (conservatively) as the 95th percentile of the aggregated data. The same method was used to compute the cross-talk factors, $\sum \overline{e_{ct}}$, for the non-moving MMs and S_m and $\sum S_{ct}$.

Considering that the modelling and numerical approximations depend on the spatial configuration of the magnets [34], the metrics in (6) from all trials were correlated with interesting distances. In particular, the Spearman correlation coefficient was calculated between each of $\overline{e_m}$, $\overline{e_{ct}}$, S_m and S_{ct}, and each of $L_{MM\text{-}sensor}$ (defined as the distance between the moving MM and the closest active site) and $L_{inter\text{-}MM}$ (defined as the distance between the moving MM and the closest MM, kept at point P_S). An additional Spearman correlation coefficient was computed between $\overline{e_{ct}}$, S_{ct}, and $L_{MMPs\text{-}sensor}$, defined as the distance between the MM kept at P_S and the closest active site.

Finally, the computation time (CT) needed to localize the MMs was measured for all the simulations, in order to

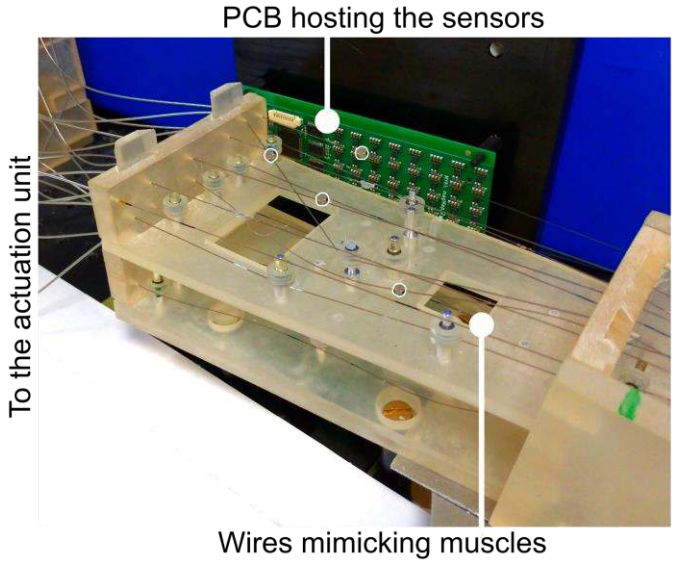

Fig. 2. The forearm mockup with *implanted* magnets. The mockup aimed at reproducing the natural position and orientation of forearm muscles, in addition to their deformation due to contraction. The mockup replicated the movements of 17 degrees of freedom of the hand and wrist, for a total of 17 wires, albeit only seven were used (only four shown in white). Muscles were modelled using a wire attached on one side to servo motors (housed in a remote actuation unit) used to actively *contract* the muscle. A grid of sensors arranged into four printed circuits boards (only one shown) surrounding the mockup were used to sample the MMs magnetic field.

investigate on the feasibility of the system to run in an online implementation. Stopwatch functions in the Matlab script were used to derive the CT of each simulation. The 95th percentile from all results was considered as the CT. The simulations ran on a desktop computer with an Intel i7-6700 CPU running at 3.4 GHz, 16 GB of RAM and Windows 7.

D. Experimental validation

A subset of the simulation results was compared with those achieved experimentally on a physical demonstrator. The latter comprised a forearm mockup, mimicking the anatomy and the contractions of the extrinsic hand muscles in humans [27], and a grid of sensors arranged into four printed circuits boards surrounding the mockup (Fig. 2). Each of the four boards was equipped with 28 sensors, spatially distributed in order to replicate the configuration of the active sites in the simulations. At this point, the readings from the sensors were stored on the PC as a baseline. Seven dMMs were then attached onto seven artificial muscles and could thus be translated along linear trajectories defined by the mockup. The magnetic field sampled by the sensors was stored for offline analysis. At the beginning of the analysis, the baseline was subtracted from these recordings so to nullify any influence on static environmental noise (including the geomagnetic field) on the performance of the localizer. In this configuration, the median $L_{MM\text{-}sensor}$, $L_{inter\text{-}MM}$ and $L_{MMPs\text{-}sensor}$, were 15.2 mm, 60 mm and 15.2 mm, respectively. Moreover, the length of the trajectories was randomly chosen between 10 mm and 20 mm (akin to the simulated ones). The same exact configuration was then replicated in the simulation environment (including electrical noise) in order to compare the performance of the two systems. In particular, the differences between the estimated trajectories from actual recordings and the simulated ones were evaluated. To do so, the real position of the MMs mounted onto the wires of the forearm mockup was estimated through CAD and physical measurements. Unfortunately, as the real orientation of the MMs could not be finely controlled, the orientation errors could not be quantified.

III. Results

The results from a representative configuration (7

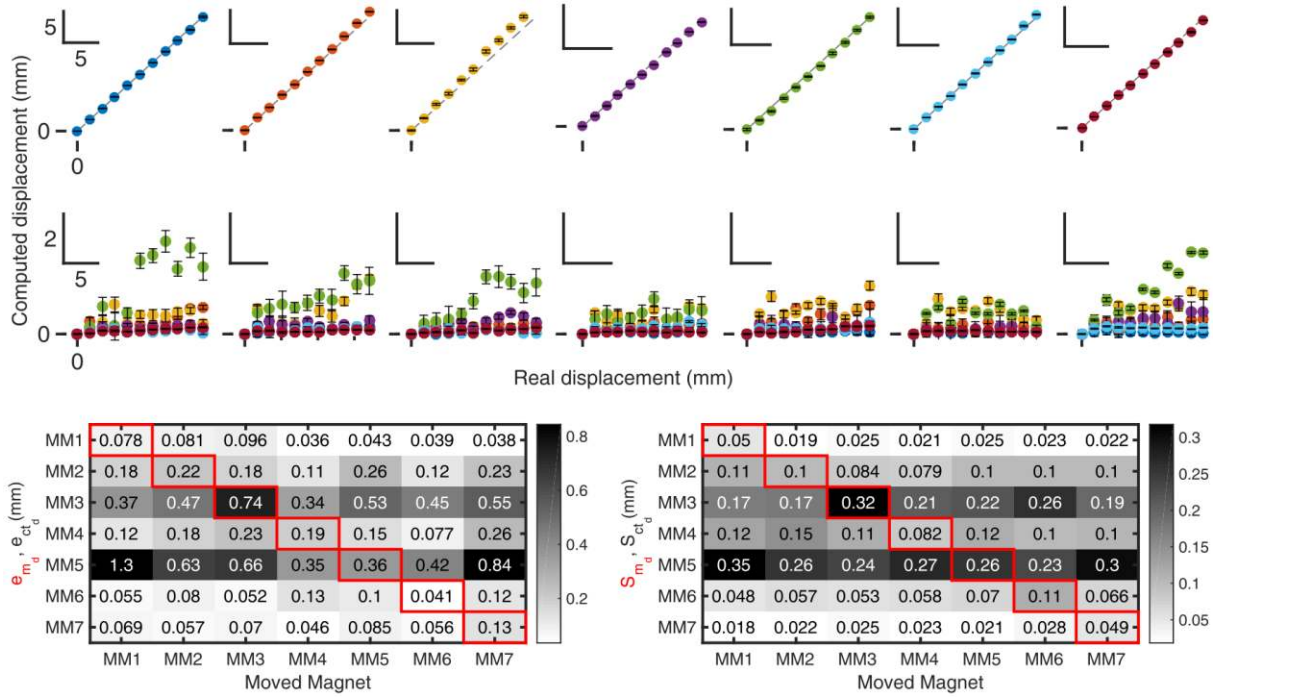

Fig. 3. Performance of the localizer in retrieving the (position) displacement of the MMs for a representative configuration (7 disc MMs, 40 sensors). Each MM was moved along a trajectory, while the remaining MMs were kept at their initial/rest position. For this configuration, the computation time (95th percentile) was 208 ms.

dMMs, 40 sensors) are first presented (Fig. 3).

The $\overline{e_m}$ was found to range between 0.3 mm and 1.8 mm across MMs (Fig. 3, lower panels). It demonstrated almost constant along the trajectory for all MMs except for MM3, where it increased with the distance from the initial position (reaching a maximum of 1.8 mm in the trajectory endpoint). The relationship between the actual and the computed displacement proved highly linear for all MMs (R^2= 0.99, p < 0.001, Fig. 3, upper panels). The movement of one MM affected the position estimate of the other MMs (Fig. 3, lower panels). The importance of this effect varied according to which MM was moved. The maximum $\overline{e_{\mathrm{ct}}}$ (1.9 mm, corresponding to 10% the length of the trajectory) was measured on the estimate of MM5 while moving MM1 (Fig. 3, lower panels).

The mean $\overline{e_m}$ (averaged across the trajectory) always proved lower than 0.74 mm (Fig. 3, lower panels, diagonal elements). This corresponds to less than 5%, of the entire trajectory of each magnet. The mean $\overline{e_{\mathrm{ct}}}$ (Fig. 3, lower panels, non-diagonal elements) proved lower than 1.3 mm, i.e. less than 10% of the entire stroke of all trajectories. The mean S_{m_d} ranged between 49 µm (MM7) and 320 µm (MM3) (Fig. 3, lower panels, diagonal elements). The mean S_{ct_d} was maximum for MM5 (and equal to 350 µm) caused by the movement of MM1. In fact, MM5 proved the magnet with higher sensibility to the movements of the other magnets (i.e. higher cross-talk) and to the variability associated to repeated measures (Fig. 3, lower panels). Conversely MM1 and MM7 proved the most immune to cross-talk and to the Gaussian noise.

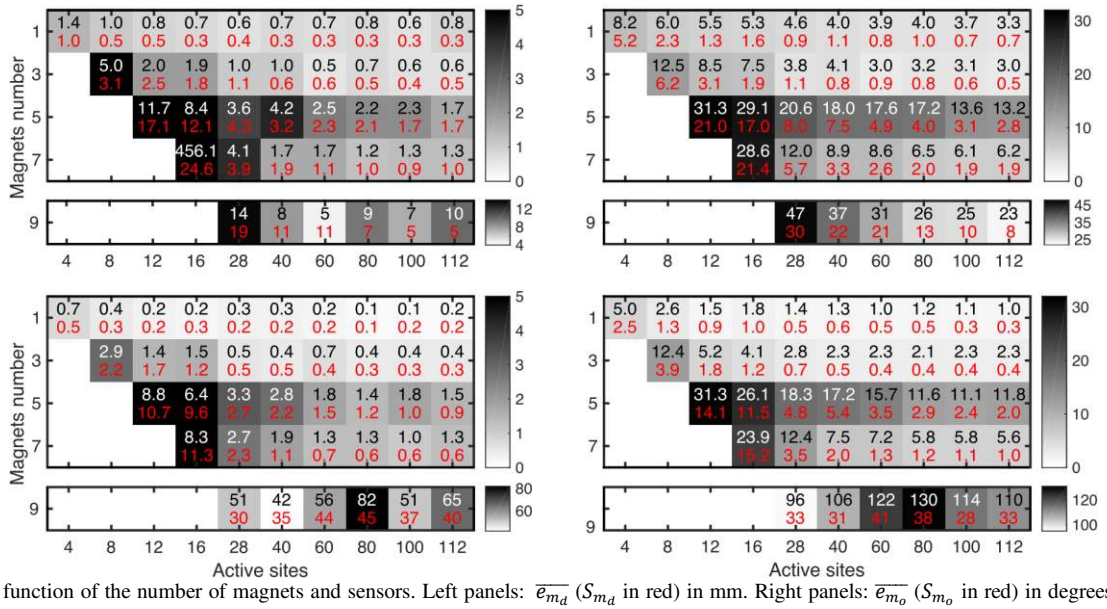

Fig. 4. $\overline{e_m}$ as a function of the number of magnets and sensors. Left panels: $\overline{e_{m_d}}$ (S_{m_d} in red) in mm. Right panels: $\overline{e_{m_o}}$ (S_{m_o} in red) in degrees. Upper panels: sphere magnets. Lower panels: disc magnets.

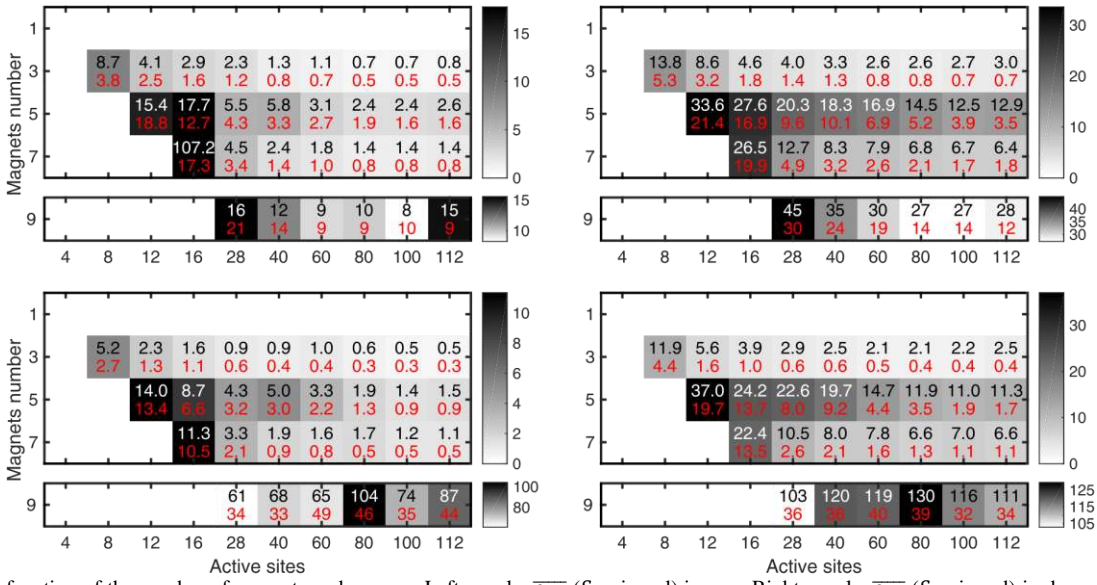

Fig. 5. $\overline{e_{ct}}$ as a function of the number of magnets and sensors. Left panels: $\overline{e_{ct_d}}$ (S_{ct_d} in red) in mm. Right panels: $\overline{e_{ct_o}}$ (S_{ct_o} in red) in degrees. Upper panels: sphere magnets. Lower panels: disc magnets.

All in all, the compound/cumulative errors increased with the number of MMs and decreased with the number of active sites (Fig. 4 and Fig. 5). E.g. the $\overline{e_m}$ for three spherical magnets decreased from 1.0 mm and 3.8° (with 28 sensors) to 0.6 mm and 3.0° (with 112 sensors); for seven magnets it decreased from 4.1 mm and 12.0° (with 28 sensors) to 1.3 mm and 6.2° (with 112 sensors) (Fig. 4, upper panels). The S_m showed similar trends and figures (Fig. 4), and the same applied for both the $\overline{e_{ct}}$ and the S_{ct_d} (Fig. 5). More pronounced improvements due to an increased number of sensors were observed with more MMs. This holds true for both the distance and orientation components (left panels vs. right panels in Fig. 4 and Fig. 5) and for both kinds of magnets (upper panels vs. lower panels in Fig. 4 and Fig. 5). The configurations with five MMs, however, showed larger errors than the seven MMs configurations. In addition, the configurations with nine MMs showed much larger errors than all other configurations. Finally, the disc magnets generally demonstrated lower errors than the spherical magnets (except for nine MMs).

The distribution of $L_{MM\text{-}sensor}$ and $L_{inter\text{-}MM}$ was affected by the number of MMs in the system (Fig. 6). Specifically, $L_{MM\text{-}sensor}$ was on average constant, whereas $L_{inter\text{-}MM}$ decreased with the number of MMs. However, the distribution of $L_{inter\text{-}MM}$ for the systems with five MMs proved similar to that with seven MMs.

The Spearman correlation analysis uncovered the relationships between the errors on the predicted displacements and the spatial configuration of the MMs and active sites (Table 2). In practice, the distances between the MMs and the closest active sites ($L_{MM\text{-}sensor}$ and $L_{MMPs\text{-}sensor}$) proved always significantly correlated with $\overline{e_m}$, $\overline{e_{ct}}$, S_m and S_{ct}, albeit these correlations exhibited a coefficient $|r| > 0.75$ only for the noise (S_m and S_{ct}) and cross-talk components ($\overline{e_{ct}}$ and S_{ct}) of the position estimates for both types of magnet (Table 2 and Fig. 7). The correlations on the orientation estimates followed the same trends (values and significances) although with lower coefficients. The correlations between the MMs inter-distances ($L_{inter\text{-}MM}$) and our metrics, proved generally negative (i.e., the larger the distance between MMs, the lower the errors). However, contrary to our expectations, they proved either irrelevant or not statistically significant (Table 2).

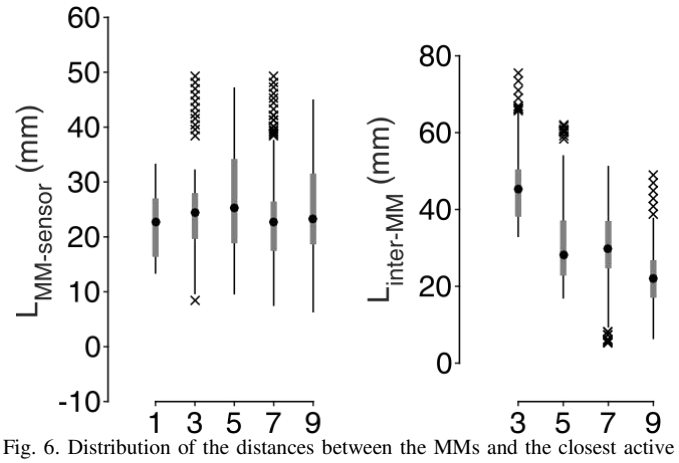

Fig. 6. Distribution of the distances between the MMs and the closest active sites ($L_{MM\text{-}sensor}$) and of the MMs inter-distances ($L_{inter\text{-}MM}$) as a function of the number of MMs.

A. *Computation time*

The CT, ranging from 6 ms (for one dMM and four sensors) to >5 s (for nine dMMs and 112 sensors), proved proportional to both the number of active sites and MMs (Fig. 8). It roughly doubled when passing from the minimum (four) to the maximum (112) number of sites, while it increased by two orders of magnitude when passing from one to nine MMs. The CT demonstrated similar between disc and spherical magnets up to seven MMs. However, for nine MMs, the CT proved larger for the discs than for the spheres, thus suggesting that the mathematical solver needed much more iterations to converge to a solution in the latter case.

B. *Experimental validation*

The positions of the seven MMs mounted on the forearm mockup were estimated using the magnetic field recorded by a matrix of 112 sensors. For the mockup, the median $\overline{e_m}$ and $\overline{e_{ct}}$ were 0.73 mm and 0.49 mm, respectively, while they proved 0.16 mm and 0.08 mm for the simulated system (Fig. 9, median difference of 0.45 and 0.3 mm). S_m and S_{ct} were comparable between the results from the forearm mockup and the simulation, being 0.017 mm and 0.015 mm for the former, and 0.015 and 0.017 for the latter, respectively (median difference smaller than 5 µm).

TABLE II

SPEARMAN CORRELATION COEFFICIENTS / P-VALUES BETWEEN THE DISPLACEMENT (PEDIX "D") AND ORIENTATION COMPONENTS (PEDIX "O") OF E_M, E_{CT}, S_M AND S_{CT} AND THE DISTANCES $L_{MM\text{-}SENSOR}$, $L_{INTER\text{-}MM}$ AND $L_{MMPS\text{-}SENSOR}$.

	sMM			dMM		
	$L_{MM\text{-}sensor}$	$L_{inter\text{-}MM}$	$L_{MMPs\text{-}sensor}$	$L_{MM\text{-}sensor}$	$L_{inter\text{-}MM}$	$L_{MMPs\text{-}sensor}$
$\overline{e_{m_d}}$	0.57 / <0.001 (a)	-0.15 / 0.012		0.41 / <0.001	0.04 / 0.506	
$\overline{e_{ct_d}}$	0.55 / <0.001 (b)	-0.12 / <0.001	0.80 / <0.001 (c)	0.49 / <0.001	-0.11 / <0.001	0.78 / <0.001
S_{m_d}	0.85 / <0.001 (d)	-0.3 / <0.001		0.83 / <0.001	-0.3 / <0.001	
S_{ct_d}	0.63 / <0.001 (e)	-0.09 / <0.001	0.87 / <0.001 (f)	0.60 / <0.001	-0.07 / <0.001	0.87 / <0.001
$\overline{e_{m_o}}$	0.57 / <0.001	-0.18 / 0.002		0.48 / <0.001	-0.19 / <0.001	
$\overline{e_{ct_o}}$	0.42 / <0.001	-0.01 / 0.65	0.66 / <0.001	0.30 / <0.001	-0.06 / 0.012	0.51 / <0.001
S_{m_o}	0.67 / <0.001	-0.26 / <0.001		0.64 / <0.001	-0.29 / <0.001	
S_{ct_o}	0.50 / <0.001	-0.15 / <0.001	0.68 / <0.001	0.49 / <0.001	-0.18 / <0.001	0.68 / <0.001

sMM and dMM refer to the spherical and disc magnets, respectively. The letters in parentheses refer to insets in Fig. 7.

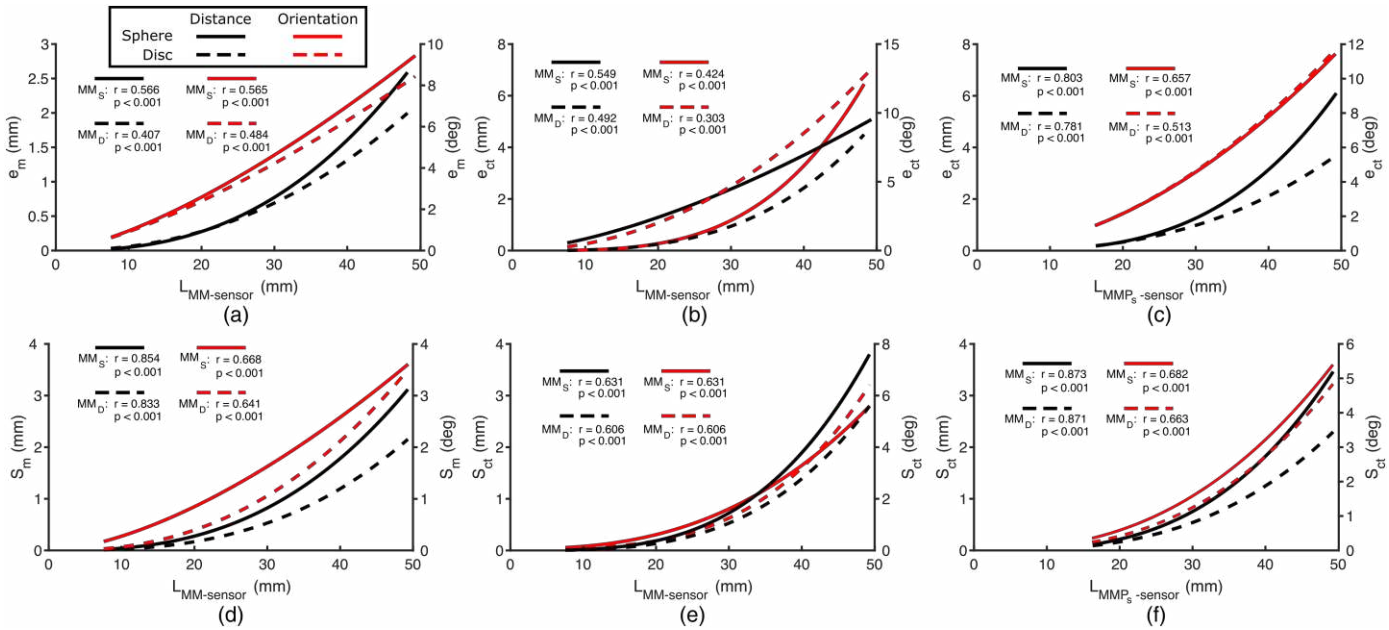

Fig. 7. Correlations between the investigated errors and interesting distances ($L_{MM\text{-}sensor}$, $L_{inter\text{-}MM}$, $L_{MMPs\text{-}sensor}$). Only the significant ($p<0.05$) and relevant ($|r| > 0.75$) correlations are shown (Table 2).

IV. Discussion

In this work, we have assessed, by simulating it, the viability and the performance of a multi-magnet localizer operating in a volume resembling the dimensions and geometries of the human forearm. By systematically varying the number of magnets to be tracked and the number of sensors used to track them, we aimed at identifying general guidelines for the design of myokinetic interfaces or, more generally, high-DoF systems operating in similar workspaces. Overall, our results confirm the information in the literature, i.e., the compound/cumulative errors increase with the number of MMs and with the distance to the sensing sites [37], and decrease with the number of sensing sites [35]. The results also add on the state of the art as our system could localize up to seven MMs, i.e., 35 DoFs, with acceptable accuracy (Fig. 4, Fig. 5, and Fig. 8). These outcomes pave the way towards the development of a transradial prosthetic hand using a myokinetic interface with up to seven implanted MMs and independent movements.

We associated the drop in performance, found with nine MMs, with the lower distance among the MMs (i.e. $L_{inter\text{-}MM}$ – Fig. 6). Interestingly, while this distance influenced the performance in a very weak manner for up to seven MMs, the degradation became particularly relevant for nine MMs as if $L_{inter\text{-}MM}$ had a step-like effect. For the MMs used in this study, the simulations suggest that this critical distance is around 30 mm. We argue that the critical distance of a generic system is strictly related with $L_{MM\text{-}sensor}$. Indeed, with decreasing $L_{inter\text{-}MM}$ distances, the localizer samples the generated magnetic field at distances that can be considered as more remote. This causes the MMs to appear to the localizer as a single magnetic dipole with a magnetic moment equal to the sum of the MMs magnetic moments. This effect can be counteracted if $L_{MM\text{-}sensor}$ decreases as well, as the localizer is provided with more local (as opposed to remote) information on the generated magnetic field. Our results suggest that the critical ratio between the two distances is around 1:1 (Fig. 6).

As all CTs were computed using a desktop PC having certain characteristics (in terms of clock rate, number of cores, etc.) and no code optimization (a Matlab script was used to localize the MMs), discussing them in absolute terms is not informative as they are linked to a non-portable implementation. This also implies that the feasibility of tracking a certain number of MMs with acceptable output rates in an embedded/portable system remains to be investigated. Nonetheless, on relative terms, we found that the CT increases exponentially with the number of MMs (Fig. 8). On the other hand, the number of active sites had a limited effect on the CT. This suggests that, depending on the system requirements, it is possible to greatly improve the performance by increasing the number of active sites, without drastically affecting the CT. We can take as an example the case of five MMs. In this case, by increasing the number of active sites from 12 to 112, the CT increased by a factor of 2.5 (from 119 to 285), but $\overline{e_{m_d}}$ and $\overline{e_{m_o}}$ decreased by a factor of seven (from 11.7 mm to 1.7 mm) and 2.5 (from 31.3 to 13.2), respectively. Thus, increasing the number of active sites is a good strategy to reduce $\overline{e_{m_d}}$. It also affects $\overline{e_{m_o}}$, but to a lower extent.

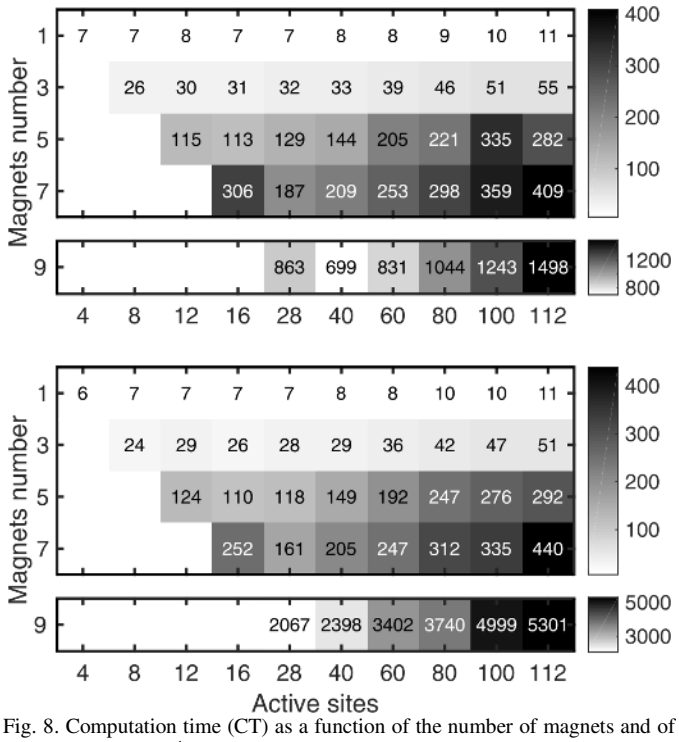

Fig. 8. Computation time (CT) as a function of the number of magnets and of active sites. The 95th percentile of the CT across the two types of simulated magnets (sphere and disc) is shown (in ms).

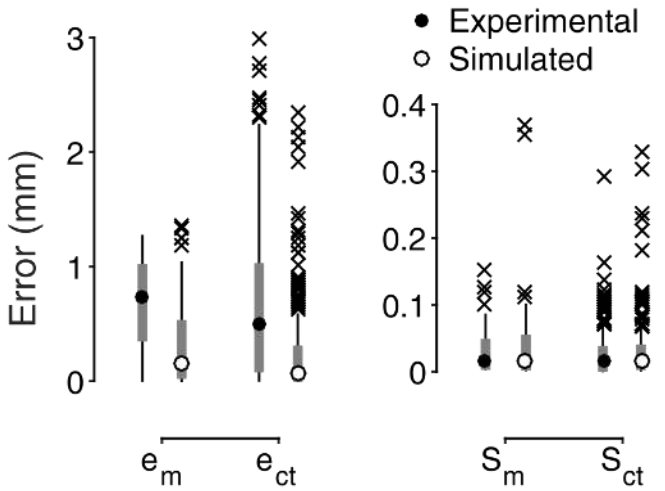

Fig. 9. Comparison of e_m, e_{ct}, S_m, S_{ct} between simulated and experimental measurements using a physical mockup (seven MMs, 112 active sites / sensors).

A different performance was observed between the two types of MM under test. In particular, the smaller MM (i.e. the sphere) generally yielded larger errors. This is probably due to the weaker magnetic field generated by that MM (magnetic moment of 0.0163 Am^2 vs. 0.029 Am^2 of the dMMs), which decreased the signal to noise ratio at the sensing site. This is also supported by the fact that, in the case of nine MMs, the simulations showed better results with the spheres, suggesting that the lower the magnetic field strength, the closer the MMs can be placed. This result was not completely obvious as the point dipole approximation better approximates the magnetic field generated by spherical magnets with respect to the one generated by discs [36]. Thus, one would expect that the localizer would perform better with spherical magnets irrespective to the distance between MMs. Our results suggest that the form factor plays a minor role in the localization performance, while the strength of and distance between MMs are the dominant factors. However, additional tests are needed in order to quantify the interplay between these factors.

Although the simulations were designed to mimic as much as possible the real system (e.g. magnets modeled as 3D objects and not as dipoles, remanent magnetization taken from experimental measurements), the experimental results did not match perfectly with them, being slightly worse (Fig. 9). This is probably the case because the real system is affected by imperfections not present in the simulated environment. Those are, for instance: the sensors position, which is not perfectly known as in the simulation, information on the real position and orientation of the MMs (based on imperfect measurements), and physical differences among MMs. Thus, our results underline the importance of testing magnetic tracking systems using a physical system. Nonetheless, the errors found in the simulation are of the same order of magnitude of the experimental ones and thus they can be used as a general guideline for the design of physical systems.

The present study was indeed limited in some respects. First, the drop in performance found with nine MMs prevented us from simulating systems with even more MMs. Then, in the experimental validation, as the mockup was fixed on a table, we also neglected any effect of the geomagnetic field on the localization performance. This was done by simply subtracting it from the measurements of the magnetic field generated by the MMs. In a physical portable system, however, the relative orientation between the localizer and the geomagnetic field would change, requiring a dynamic rejection of this disturbance. As an example, this may be implemented using a differential model [40], or through a remote sensor. Additionally, in order to limit the number of combinations tested, a few parameters/assumptions were set/made a priori. For instance, the initial guess of the pose required by the Levenberg-Marquardt algorithm to solve (3) was set as the true pose of the MMs. This is an ideal situation that is not present in an online system, where the true pose is not available. Specific algorithms that allow precise estimations of the initial guess exist (e.g. particle swarm optimization [35]) but the sensitivity of the Levenberg-Marquardt algorithm to the quality of the initial guess still remains to be quantified. On another note, the active sites were placed on a 9 mm step grid. This apparently arbitrary parameter was set having in mind the physical system. Specifically, this distance was set as a trade-off between the size of the physical sensors and the size of the workspace to track. The former would have allowed to place the active sites even closer to each other (at around 5 mm distance), while the latter demanded for a larger distance between them to limit the total number of active sites. Moreover, the active sites in the different configurations were picked depending on the measured strength of the magnetic field. Although this method globally increases the signal to noise ratio and should thus improve the performance of the localizer [22], [37], other strategies [1], [37] could have been used instead. Finally, magnets were moved one at a time in

both the simulations and experimental validation. Although this may be perceived as a limitation, it was required in order to correctly compute $\overline{e_m}$ and $\overline{e_{ct}}$. However, as all tests were basically static (the localizer retrieved the position of MMs fixed in a certain position), moving one or more MMs would have only generated different static configurations of the MMs. Thus, as these were randomly generated in the first place, we have no reason to think that moving more MMs at the same time would have significantly affected the performance of the system. On the other hand, it remains to be tested if the dynamic performance of the localizer (i.e. the ability to retrieve the position of moving MMs) would differ consistently from the present results. This becomes of pivotal importance in systems using a large number of sensors, requiring long times to sample the data.

V. Conclusion

A systematic evaluation of the number of magnets to be tracked and the number of sensors used to track them allowed us to formulate general guidelines for the implementation of magnetic tracking systems. Our results are in line with previous findings, and suggest that (i) the pose estimation error increases with the number of MMs and (ii) decreases with the number of active sites; (iii) the computation time is greatly influenced by the number of MMs to localize, while it is (iv) less influenced by the number of active sites used; finally, (v) the MMs position estimation error is more influenced by the number of active sites used than the orientation estimation error.

References

[1] O. Talcoth and T. Rylander, "Optimization of sensor positions in magnetic tracking," *Chalmers University of Technology*. Gothenburg, pp. 1–30, 2011.

[2] D. A. Robinson, "A Method of Measuring Eye Movement Using a Scleral Search Coil in a Magnetic Field," *IEEE Trans. Bio-Medical Electron.*, vol. 10, no. 4, pp. 137–145, 1963.

[3] H. Collewijn, F. van der Mark, and T. C. Jansen, "Precise recording of human eye movements," *Vision Res.*, vol. 15, no. 3, 1975.

[4] H. L. Payne and J. L. Raymond, "Magnetic eye tracking in mice," *Elife*, vol. 6, pp. 1–24, 2017.

[5] J. M. Gilbert *et al.*, "Isolated word recognition of silent speech using magnetic implants and sensors," *Med. Eng. Phys.*, vol. 32, no. 10, pp. 1189–1197, 2010.

[6] F. H. Raab, E. B. Blood, T. O. Steiner, and H. R. Jones, "Magnetic Position and Orientation tracking system," *IEEE Trans. Aerosp. Electron. Syst.*, vol. AES-15, no. 5, pp. 709–718, 1979.

[7] S. Yabukami *et al.*, "A new tracking system of jaw movement using two magnets," *IEEE Trans. Magn.*, vol. 38, no. 5 I, pp. 3315–3317, 2002.

[8] J. T. Sherman, J. K. Lubkert, R. S. Popovic, and M. R. DiSilvestro, "Characterization of a novel magnetic tracking system," *IEEE Trans. Magn.*, vol. 43, no. 6, pp. 2725–2727, 2007.

[9] E. J. Rouse, D. C. Nahlik, M. A. Peshkin, and T. A. Kuiken, "Development of a Model Osseo-Magnetic Link for Intuitive Rotational Control of Upper-Limb Prostheses," *IEEE Trans. Neural Syst. Rehabil. Eng.*, vol. 19, no. 2, pp. 213–220, Apr. 2011.

[10] T. Penzkofer *et al.*, "Free-hand CT-based electromagnetically guided interventions: Accuracy, efficiency and dose usage," *Minim. Invasive Ther. Allied Technol.*, vol. 20, no. 4, pp. 226–233, Jul. 2011.

[11] J. Krücker *et al.*, "Electromagnetic Tracking for Thermal Ablation and Biopsy Guidance: Clinical Evaluation of Spatial Accuracy," *J. Vasc. Interv. Radiol.*, vol. 18, no. 9, pp. 1141–1150, 2007.

[12] S. Krueger, H. Timinger, R. Grewer, and J. Borgert, "Modality-integrated magnetic catheter tracking for x-ray vascular interventions," *Phys. Med. Biol.*, vol. 50, no. 4, pp. 581–597, 2005.

[13] S. Leong *et al.*, "Electromagnetic navigation bronchoscopy: A descriptive analysis," *J. Thorac. Dis.*, vol. 4, no. 2, pp. 173–85, Apr. 2012.

[14] S. G. Shah, B. P. Saunders, J. C. Brooker, and C. B. Williams, "Magnetic imaging of colonoscopy: An audit of looping, accuracy and ancillary maneuvers," *Gastrointest. Endosc.*, vol. 52, no. 1, pp. 1–8, Jul. 2000.

[15] N. M. Prakash and F. A. Spelman, "Localization of a magnetic marker for GI motility studies: an in vitro feasibility study," in *Engineering in Medicine and Biology Society, 1997. Proceedings of the 19th Annual International Conference of the IEEE*, 1997, vol. 6, pp. 2394–2397.

[16] M. Salerno *et al.*, "A discrete-time localization method for capsule endoscopy based on on-board magnetic sensing," *Meas. Sci. Technol.*, vol. 23, no. 1, 2012.

[17] K. Yu, G. Fang, and E. Dutkiewicz, "Position and Orientation Accuracy Analysis for Wireless Endoscope Magnetic Field Based Localization System Design," in *2010 IEEE Wireless Communication and Networking Conference*, 2010, pp. 1–6.

[18] X. Wang, M. Q. H. Meng, and C. Hu, "A localization method using 3-axis magnetoresistive sensors for tracking of capsule endoscope," *Proc. Annu. Int. Conf. IEEE Eng. Med. Biol.*, vol. 1, no. 3, pp. 2522–2525, 2006.

[19] D. Pham and S. M. Aziz, "A Real-Time Localization System for an Endoscopic Capsule Using Magnetic Sensors," *Sensors*, vol. 14, no. 11, pp. 20910–20929, 2014.

[20] W. Andrä *et al.*, "A novel method for real-time magnetic marker monitoring in the gastrointestinal tract," *Phys. Med. Biol.*, vol. 45, no. 10, pp. 3081–3093, 2000.

[21] C. Hu *et al.*, "Locating Intra-Body Capsule Object by Three-Magnet Sensing System," *IEEE Sens. J.*, vol. 16, no. 13, pp. 5167–5176, Jul. 2016.

[22] C. Hu, T. Ma, and M. Q.-H. Meng, "Sensor Arrangement Optimization of Magnetic Localization and Orientation system," in *2007 IEEE International Conference on Integration Technology*, 2007, pp. 311–315.

[23] V. Pasku *et al.*, "Magnetic Field-Based Positioning Systems," *IEEE Commun. Surv. Tutorials*, vol. 19, no. 3, pp. 2003–2017, 2017.

[24] T. M. Peters and K. R. Cleary, *Image-guided interventions: technology and applications*. Springer, 2008.

[25] A. M. Franz, T. Haidegger, W. Birkfellner, K. Cleary, T. M. Peters, and L. Maier-Hein, "Electromagnetic Tracking in Medicine - A Review of Technology, Validation, and Applications," *IEEE Trans. Med. Imaging*, vol. 33, no. 8, pp. 1702–1725, Aug. 2014.

[26] V. Schlageter, P.-A. Besse, R. S. Popovic, and P. Kucera, "Tracking system with five degrees of freedom using a 2D-array of Hall sensors and a permanent magnet," *Sensors Actuators A Phys.*, vol. 92, no. 1–3, pp. 37–42, 2001.

[27] S. Tarantino, F. Clemente, D. Barone, M. Controzzi, and C. Cipriani, "The myokinetic control interface: tracking implanted magnets as a means for prosthetic control," *Sci. Rep.*, vol. 7, no. 1, p. 17149, 2017.

[28] "The MYKI project website." [Online]. Available: http://www.mykierc.eu/.

[29] P. A. Parker, K. B. Englehart, and B. Hudgins, "Myoelectric signal processing for control of powered limb prostheses," *J. Electromyogr. Kinesiol.*, vol. 16, no. 6, pp. 541–548, 2006.

[30] G. A. DeMichele, Z. Hu, P. R. Troyk, H. Chen, and R. F. ff. Weir, "Low-power polling mode of the next-generation IMES2 Implantable wireless EMG sensor," in *36th Annual International Conference of the IEEE Engineering in Medicine and Biology Society*, 2014, pp. 3081–3084.

[31] R. F. ff. Weir, P. R. Troyk, G. A. DeMichele, D. A. Kerns, J. F. Schorsch, and H. Maas, "Implantable Myoelectric Sensors (IMESs) for Intramuscular Electromyogram Recording," *IEEE Trans. Biomed. Eng.*, vol. 56, no. 1, p. 2009, 2009.

[32] P. F. Pasquina *et al.*, "First-in-man demonstration of a fully implanted myoelectric sensors system to control an advanced electromechanical prosthetic hand," *J. Neurosci. Methods*, vol. 244, pp. 85–93, 2015.

[33] C. Hu, M. Q.-H. Meng, and M. Mandal, "Efficient Linear Algorithm

for Magnetic Localization and Orientation in Capsule Endoscopy," *Eng. Med. Biol. Soc. 2005. IEEE-EMBS 2005. 27th Annu. Int. Conf.*, vol. 2, no. 1, pp. 7143–7146, 2005.

[34] S. Yabukami *et al.*, "Motion capture system of magnetic markers using three-axial magnetic field sensor," *IEEE Trans. Magn.*, vol. 36, no. 5, pp. 3646–3648, 2000.

[35] W. Yang, C. Hu, M. Li, M. Q.-H. Meng, and S. Song, "A new tracking system for three magnetic objectives," *IEEE Trans. Magn.*, vol. 46, no. 12, pp. 4023–4029, 2010.

[36] M. N. O. Sadiku, *Elements of electromagnetics*, 5th ed. Oxford University Press, 2014.

[37] L. Maréchal, S. Foong, S. Ding, K. L. Wood, V. Patil, and R. Gupta, "Design Optimization of a Magnetic Field-Based Localization Device for Enhanced Ventriculostomy," *J. Med. Device.*, vol. 10, no. 1, p. 011006, 2016.

[38] T. M. Greiner, "Hand Anthropometry of U.S. Army Personnel," *Technical Report*. United States Army Natick Research, Development and Engineering Center, Natick, pp. 1–434, 1991.

[39] D. W. Marquardt, "An Algorithm for Least-Squares Estimation of Nonlinear Parameters," *J. Soc. Ind. Appl. Math.*, vol. 11, no. 2, pp. 431–441, 1963.

[40] X. Huo, J. Wang, and M. Ghovanloo, "A wireless tongue-computer interface using stereo differential magnetic field measurement," *Eng. Med. Biol. Soc. (EMBC), 2007 Annu. Int. Conf. IEEE*, pp. 5723–5726, 2007.